Absorptive lasing mode suppression in ZnO nano- and microcavities

M. Wille, T. Michalsky, E. Krüger, M. Grundmann, and R. Schmidt-Grund

Citation: Appl. Phys. Lett. **109**, 061102 (2016); doi: 10.1063/1.4960660
View online: https://doi.org/10.1063/1.4960660
View Table of Contents: http://aip.scitation.org/toc/apl/109/6
Published by the American Institute of Physics

Absorptive lasing mode suppression in ZnO nano- and microcavities

M. Wille, T. Michalsky, E. Krüger, M. Grundmann, and R. Schmidt-Grund
Universität Leipzig, Institut für Experimentelle Physik II, Linnéstraße 5, 04103 Leipzig, Germany

(Received 19 May 2016; accepted 28 July 2016; published online 8 August 2016)

We conclusively explain the different lasing mode energies in ZnO nano- and microcavities observed by us and reported in literature. The limited penetration depth of usually used excitation lasers results in an inhomogeneous spatial gain region depending on the structure size and geometry. Hence, weakly or even nonexcited areas remain present after excitation, where modes are instantaneously suppressed by excitonic absorption. We compare the effects for ZnO microwires, nanowires, and tetrapod-like structures at room temperature and demonstrate that the corresponding mode selective effect is most pronounced for whispering-gallery modes in microwires with a hexagonal cross section. Furthermore, the absorptive lasing mode suppression will be demonstrated by correlating the spot size of the excitation laser and the lasing mode characteristic of a single ZnO nanowire. *Published by AIP Publishing.* [http://dx.doi.org/10.1063/1.4960660]

Zinc oxide (ZnO) is an efficient emitter for near ultraviolet (NUV) light, making it a promising material for future optoelectronic applications. The investigation of stimulated emission in ZnO micro- and nanostructures is in the focus of the last few years' research. The goal is to achieve light emitting building blocks with a diverse functionality and the ability of easy integration in complex circuits. In fact, ZnO micro- and nanostructures provide all components necessary for laser action: Under sufficiently high excitation, the semiconductor material provides gain and the respective structures represent different resonator types due to their geometry. Single nanowires, i.e., act as Fabry-Pérot resonator due to reflections at the end facets,[1] whereas a closed round trip of modes within the hexagonal cross section of microwires mediated by total internal reflection provides a whispering gallery type resonator.[2] Tetrapod-like nanoparticles may also exhibit lasing, whereby the resonator structure is provided by multiple reflections in the tetrapod legs similar to a Fabry-Pérot type resonator.[3,4] However, the tunability of the laser mode energy over a wide spectral range is a key requirement for laser applications. A variety of approaches like spatial composition gradients in $In_xGa_{1-x}N$[5] and CdS_xSe_{1-x} (Ref. 6) resonators were applied to tackle this issue, with remarkable progress for ensemble structures. However, the mode energy tunability of single micro- and nanostructures is still in the focus of current research. Besides the tunability, lasing modes in ZnO micro- and nanostructures were observed in different spectral ranges without a conclusive explanation about the observed mode energy.[7–13]

The aim of this work is to study the influence of the excitation conditions in correlation with the size and geometry of the active medium on the laser mode energy. Therefore, we compare the lasing mode energies of different single micro- and nanostructures, and discuss the results in terms of the spatial gain region, which results from the spatial inhomogeneity of the excitation spot and the limited penetration depth of the exciting laser light. For the qualitative discussion of lasing mode energies in different structures, carrier density dependent refractive index calculations will be presented. Furthermore, the concept of absorptive lasing mode suppression will be proven by the dependence of the lasing mode energies of a single ZnO nanowire on the excitation spot diameter.

ZnO nanowires with diameters in the range of $100-400$ nm and lengths up to $50\,\mu$m were synthesized by a chemical vapour deposition (CVD) process using the vapour-liquid-solid (VLS) mechanism.[14] For further details of the nanowire growth process, see Ref. 15. Microwires and nanoparticles of ZnO were synthesized using a carbothermal evaporation method under controlled ambient conditions, where both structure types grow simultaneously on a target consisting of ZnO and carbon (mass ratio 1:1). The furnace temperature, pressure, and growth time were set to 1100 °C, 120 mbar and 30 min. After the growth process, the nano- and microstructures were transferred onto a clean SiO_2/Si substrate by dry imprint technique for subsequent spatially resolved micro photoluminescence (μ-PL) measurements. The thermally grown low refractive index SiO_2 layer (thickness of $1.5\,\mu$m) ensures strong optical mode confinement in the nanowire waveguide by avoiding leakage of the electromagnetic field into the substrate and hence the energy dissipation out of the nanowire optical cavity.[16] Figure 1(a) depicts scanning electron microscope (SEM) images of an exemplary nanowire, microwire, and tetrapod-like nano particle investigated in this study. A frequency doubled Ti:Sapphire laser ($\lambda_{ex} = 355$ nm $t_{pulse} = 2$ ps, $f_{rep} = 76$ MHz) was focused by a $50\times$ NUV microscope objective (NA = 0.4) to a spot size of $10-50\,\mu m^2$ for non-resonant and variable spatial excitation of different nano- and microstructures. A variable attenuator was used to adjust the excitation power density. The luminescence light was collected by the same objective, dispersed by a spectrometer (320 mm focal length, 2400 grooves/mm grating) and detected by a Peltier-cooled, back-illuminated CCD camera with a spectral resolution of $\sim 500\,\mu$eV. The laser power was measured using a Si diode power meter.

Figure 1(b) depicts the room temperature emission spectra for different excitation powers of three different micro- and nanostructures which are shown in Fig. 1(a). All three structures exhibit lasing under high excitation powers, which was proven by investigating the integrated PL intensity versus the excitation power (not shown here). Obviously, the

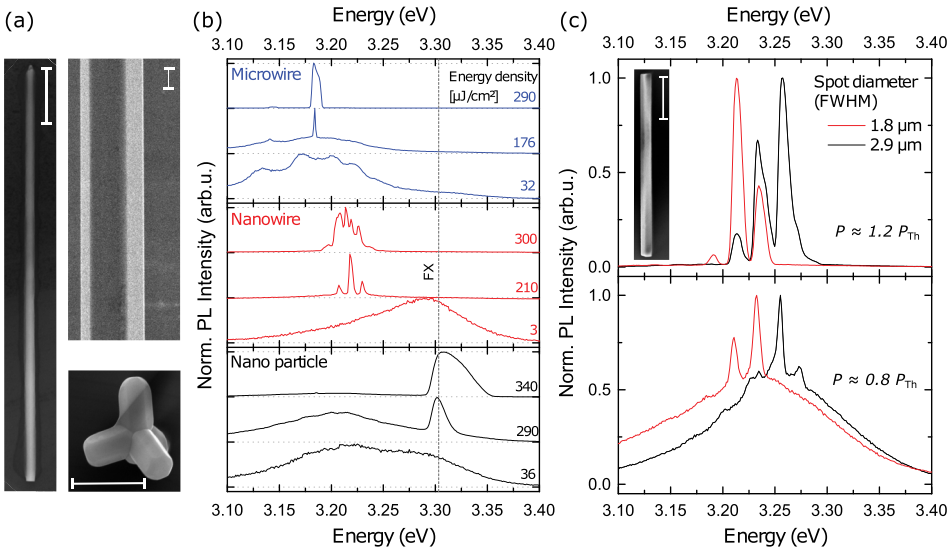

FIG. 1. (a) Scanning electron microscope images (SEM) of a ZnO nanowire (length 7.9 μm, diameter 165 – 190nm), microwire (diameter 3.5 μm), and a tetrapod-like nano particle (leg length of ~800nm and leg diameter of ~450nm). The white bars have a length of 1 μm. (b) Room temperature PL spectra (linear scale) for three different structure types and three excitation powers reveal lower lasing mode energies for larger structure dimensions. (c) Lasing emission spectra of a ZnO nanowire (see inset: length 4.2 μm, diameter 245nm), shown for two excitation spot diameters of 1.8 μm (red) and 2.9 μm (black). The excitation with a larger spot size leads to a mode enhancement on the high energy side of the spectrum.

lasing mode emission energies of the micro- and nanostructures are different. For the investigated exemplary microwire with a diameter of 3.5 μm and a laser threshold power of $P_{Th} \sim 180\,\mu J/cm^2$, the mode energy is around 3.18 eV (see blue spectra in Fig. 1(b)). At even higher excitation powers, additional modes appear on the low energy side of the main emission. The lasing emission from a single ZnO nanowire with a length of 7.9 μm and a diameter of 180 nm (red spectra in Fig. 1(b)) emerges at energies between 3.19 eV and 3.23 eV, with a respective laser threshold power of $P_{Th} \sim 190\,\mu J/cm^2$. Also here, with increasing excitation power in the lasing regime, further modes emerge on the low energy side of the spectra. The tetrapod-like particle, however, exhibits lasing emission ($P_{Th} \sim 270\,\mu J/cm^2$) at around 3.30 eV, which continuously broadens to the high energy side up to 3.35 eV with increasing excitation power (see black spectra in Fig. 1(b). Note that the emission energy of the nano particle is similar to that of the free exciton emission. However, it will be shown below that optical gain is provided by an electron-hole plasma (EHP) in all investigated nano- and microstructures. These emission characteristics are typical for the respective resonator types and, as mentioned above, are also observed in literature. The observed lasing threshold powers for all structures are similar. Thus, energy shifts due to varying carrier densities and accompanying renormalization effects can be excluded in our experiment. Furthermore, the emission energy of single nanowires was found to be slightly tunable by changing the spot size of the excitation laser. Figure 1(c) depicts the lasing emission spectra of a ~4.2 μm long nanowire (see inset) slightly below and above the respective threshold power for different excitation spot sizes (red for ~1.8 μm and black for ~2.9 μm). Note that additional modes appear on the high energy side of the spectra in the case of a larger excitation spot (black lines).

The different lasing mode energies of the respective micro- and nanostructures can be well explained by considering the spectral gain profile of the semiconductor material under high excitation and the spatial distribution of electronically inverted regions in the respective structures. The complex refractive index, calculated by means of solving the Bethe-Salpeter ladder equation with a matrix inversion method,[15] is depicted in Fig. 2(a) for carrier concentrations of $1 \times 10^{15} cm^{-3}$ and $5 \times 10^{19} cm^{-3}$ which represent the cases of excitation far below and slightly above the Mott density. The excitonic resonance/absorption, visible as pronounced peak for low carrier concentration, vanishes at high carrier concentrations, accompanied by the formation of optical gain for energies between 3.1 eV and 3.35 eV. The calculations are based on the treatment of an EHP without any excitonic screening. In contrast to competitive gain processes like exciton-exciton, exciton-carrier, and exciton-phonon scattering, only the gain provided by an EHP is high enough to overcome the resonator losses of the investigated nano- and microstructures at room temperature. To obtain further insight into the carrier density dependent complex refractive index and its temporal dynamics after a strong excitation pulse, the reader is referred to Ref. 15. The spectral gain range is shown magnified in Fig. 2(c). Each of the differently highlighted areas represents a variety of experimentally observed lasing energies for the respective microwires,[10,11] nanowires/nanobelts,[7,13] and nanoparticles/tetrapods,[3,8] as indicated in Fig. 2(c). Obviously, particles of smaller size exhibit lasing modes with higher energies compared to several μm-long nanowires and μm-thick microwires.

This behavior can be explained by considering the spatial absorption profile of the excitation laser light in the respective structures, see Fig. 2(b). Due to the confocal excitation, microwires are only excited at the side facing the excitation laser. The limited penetration depth (~65 nm at 355 nm) and carrier diffusion with a typical diffusion length of 0.25–0.50 μm[17,18] lead to a weakly or even non-excited microwire backside. This leads to absorption conditions outside of the transparency region (above ~3.2 eV). Hence, as whispering-gallery modes (WGMs) are the resonant modes in microwires which travel throughout the entire wire cross section, only WGM with energies below ~3.2 eV can be observed. In this energy range, the accessible gain is comparatively low, which leads to a higher threshold power for lasing in microwires. Furthermore, these WGMs are totally reflected at the inner hexagonal side walls. Hence, cavity

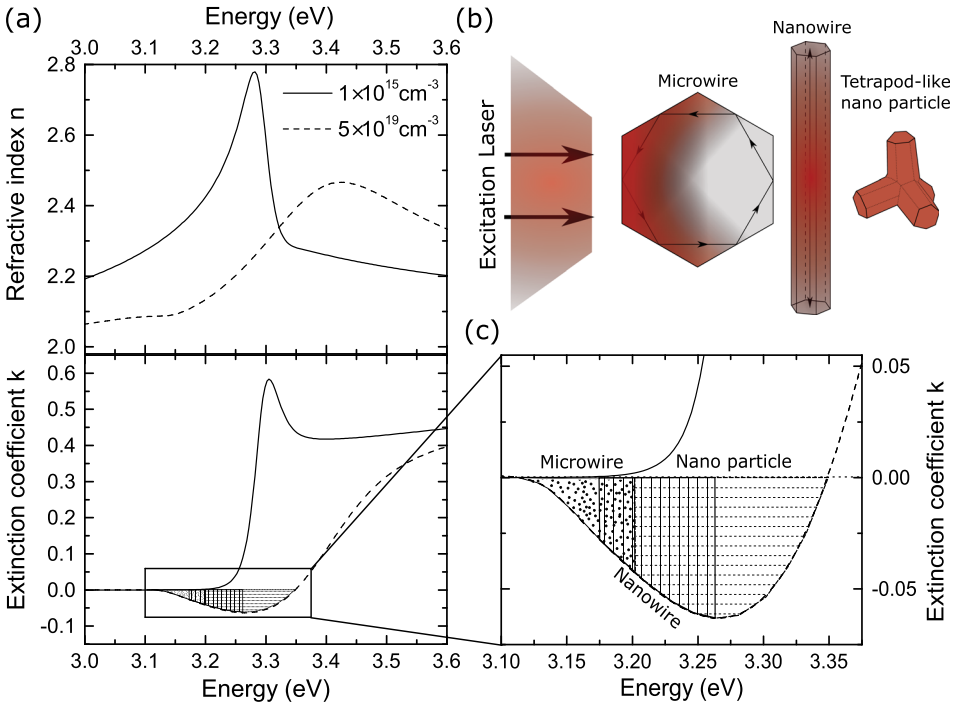

FIG. 2. (a) Calculated carrier density dependent complex refractive index for 1×10^{15} cm^{-3} (solid line) and 5×10^{19} cm^{-3} (dashed line). (b) Sketch of the spatial gain regions in different nano- and microstructures (microwire, nanowire, and nanoparticle) under excitation with a Gaussian laser profile. Red color indicates high carrier densities and thus high gain whereas white color indicates regions without any excited carriers. (c) Sketch of differently hatched energy ranges in the enlarged gain spectra for a carrier density of 5×10^{19} cm^{-3}, for which lasing was observed for different nano- and microstructures in literature.

losses are negligible compared to the absorption losses connected to the inhomogeneous carrier distribution. In the case of nanowire lasing, experimentalists commonly try to excite the nanowires with a typical length of 4–20 μm homogeneously over its entire length. However, due to the Gaussian profile of the excitation laser spot, the end facet near regions of the nanowire are less strongly excited compared to the center of the nanowire (see color gradient in Fig. 2(b)). If the carrier density in the weaker excited region is below the Mott density, excitonic absorption leads to the absence of modes on the high energy side of the gain profile. In contrast to microwires, the resonant Fabry-Pérot modes in nanowires are reflected at the facet ends with a reflectivity of around 20% – 50 % (Ref. 13) causing a higher laser threshold power. Hence, cavity losses have a significant influence on the emission characteristics. To prove the influence of the inhomogeneous carrier distribution on the emission characteristics of nanowires, we fixed the cavity loss by using the same nanowire and varied the spot size of the excitation laser. As a result, the ratio of excited to non-excited nanowire volume can be varied. This experiment was performed for a 4.2 μm long nanowire with spot sizes of 1.8 μm and 2.9 μm (see Fig. 1(c)). A larger spot size leads to a more homogeneous carrier density distribution along the nanowire and thus to less absorption in the regions close to the end facets. Therefore, additional modes on the high energy side of the lasing spectra can be observed in contrast to the spectra recorded with a smaller spot size. For nanoparticles with a maximum extension of $\lesssim$3 μm, carrier diffusion leads to a homogeneous gain distribution in the semiconductor material. The cavity losses are again dominated by the low mode reflectivity at the leg facets. To overcome these cavity losses in a nanoparticle, even higher pump densities are necessary because of the smaller active resonator. Hence, only lasing modes with energies in the spectral vicinity of the gain profile maximum are amplified in the nanoparticle. Figure 2(c) depicts the maximum of the gain profile at around 3.27 eV and the presence of gain up to 3.35 eV, which explains the high energy lasing mode emission of the tetrapod-like particle in Fig. 1(b) quite well.

Furthermore, we found that in the lasing regime the time integrated peaks are broader for smaller structure sizes (see Fig. 1(b)). This is most likely a direct consequence of the short excitation pulse and of the fact that in a smaller cavity a larger fraction of the cavity length is excited. The short excitation pulse creates a reservoir of carriers with high density which decays on the time scale of several picoseconds. This leads to a temporal red shift $\Delta\lambda$ of the lasing modes after excitation and results in a peak broadening in time integrated PL experiments.[15] Additionally, the higher cavity losses for smaller structures like for shorter nanowires (see Fig. 1(c)) and tetrapods may also contribute to the linewidth increase of the lasing modes. However, this influence is expected to be small compared to the modal energy shift after the ultrafast excitation.

In lasing experiments on single micro- and nanostructures, the respective lasing mode energy was found to depend strongly on the excitation conditions in terms of spatial distribution of the excited structure region and on the resonator geometry. Depending on the structure size, a certain structure volume remains weakly or even non-excited after excitation. This leads to mode absorption outside of the spatial gain region. For hexagonal microwires with diameters of several microns, the effect is most pronounced due to the small gain region close to the front facet. In the case of lasing nanoparticles, the carrier concentration is spatially homogeneous. Hence, gain distribution correlated absorption effects are negligible and lasing modes are observable on the high energy side of the gain profile. Nanowires behave in an intermediate fashion due to the weaker excitation in the end facet near region. By changing the spot size, the length of absorbing end facet region was varied. As a consequence, we

observed lasing modes on the high energy side of the emission spectra in the case of homogeneous carrier density distribution, i.e., larger spot size. For a smaller spot size, high energy lasing modes are suppressed outside of the transparency region.

This work was supported by the Deutsche Forschungsgemeinschaft within Gr 1011/26-1, the "Leipzig Graduate School of Natural Sciences—BuildMoNa" and through FOR1616. We thank C. Sturm and S. Richter for valuable discussions.

[1]J. Johnson, H. Yan, P. Yang, and R. Saykally, J. Phys. Chem. B **107**, 8816 (2003).
[2]C. Czekalla, C. Sturm, R. Schmidt-Grund, B. Cao, M. Lorenz, and M. Grundmann, Appl. Phys. Lett. **92**, 241102 (2008).
[3]J. M. Szarko, J. K. Song, C. W. Blackledge, I. Swart, S. R. Leone, S. Li, and Y. Zhao, Chem. Phys. Lett. **404**, 171 (2005).
[4]L. E. Li and L. N. Demianets, Opt. Mater. **30**, 1074 (2008).
[5]T. Kuykendall, P. Ulrich, S. Aloni, and P. Yang, Nat. Mater. **6**, 951 (2007).
[6]A. Pan, W. Zhou, E. Leong, R. Liu, A. H. Chin, B. Zou, and C. Ning, Nano Lett. **9**, 784 (2009).
[7]Z. Qiu, K. Wong, M. Wu, W. Lin, and H. Xu, Appl. Phys. Lett. **84**, 2739 (2004).
[8]H. Cao, J. Xu, E. Seelig, and R. Chang, Appl. Phys. Lett. **76**, 2997 (2000).
[9]D. Yu, Y. Chen, B. Li, X. Chen, M. Zhang, F. Zhao, and S. Ren, Appl. Phys. Lett. **91**, 091116 (2007).
[10]J. Dai, C. Xu, K. Zheng, C. Lv, and Y. Cui, Appl. Phys. Lett. **95**, 241110 (2009).
[11]R. Chen, B. Ling, X. W. Sun, and H. D. Sun, Adv. Mater. **23**, 2199 (2011).
[12]T. Michalsky, M. Wille, C. Dietrich, R. Röder, C. Ronning, R. Schmidt-Grund, and M. Grundmann, Appl. Phys. Lett. **105**, 211106 (2014).
[13]M. Zimmler, F. Capasso, S. Müller, and C. Ronning, Semicond. Sci. Technol. **25**, 024001 (2010).
[14]R. Wagner and W. Ellis, Appl. Phys. Lett. **4**, 89 (1964).
[15]M. Wille, C. Sturm, T. Michalsky, R. Röder, C. Ronning, R. Schmidt-Grund, and M. Grundmann, Nanotechnology **27**, 225702 (2016).
[16]R. Röder, M. Wille, S. Geburt, J. Rensberg, M. Zhang, J. G. Lu, F. Capasso, R. Buschlinger, U. Peschel, and C. Ronning, Nano Lett. **13**, 3602 (2013).
[17]A. Soudi, P. Dhakal, and Y. Gu, Appl. Phys. Lett. **96**, 253115 (2010).
[18]O. Lopatiuk, L. Chernyak, A. Osinsky, J. Xie, and P. Chow, Appl. Phys. Lett. **87**, 214110 (2005).